



Soil carbon mineralization and microbial community dynamics in response to pyrogenic organic matter addition

Nayela Zeba^{a,*}, Timothy D. Berry^a, Monika S. Fischer^b, Matthew F. Traxler^b, Thea Whitman^a

^a Department of Soil Science, University of Wisconsin-Madison, 1525 Observatory Dr., Madison, WI, 53706, USA

^b Department of Plant and Microbial Biology, University of California, Berkeley, 111 Koshland Hall, Berkeley, CA, 94720, USA

ARTICLE INFO

Keywords:

Pyrogenic organic matter
Biochar
Mineralization
Priming
Bacteria and fungi

ABSTRACT

Wildfires can either negatively impact soil carbon (C) stocks through combustion or increase soil carbon stocks through the production of pyrogenic organic matter (PyOM), which is highly persistent and can affect non-pyrogenic soil organic carbon (SOC) mineralization rates. In this study, we used fine-resolution ¹³C₂ flux tracing to investigate PyOM-C mineralization, soil priming effects, and their impacts on soil microbial communities in a Californian mixed conifer forest Xerumbrept soil burned in the 2014 King Fire. We added PyOM produced from pine biomass at 350 °C and 550 °C to the soil and separately traced the mineralization of ¹³C-labeled water-extractable and non-water-extractable PyOM-C fractions in a short-term 30-day incubation.

Our results indicate that at the end of the incubation period, the water-extractable fraction was 10–50x more mineralizable in both 350 °C and 550 °C PyOM treatments than the SOC or non-water-extractable PyOM fraction. The addition of 350 °C PyOM led to a short-term positive priming effect, likely due to co-metabolism of easily mineralizable PyOM-C and the SOC, whereas 550 °C PyOM addition induced negative priming, potentially due to physical protection of SOC. We observed significant shifts in bacterial community composition in response to both 350 °C and 550 °C PyOM, and identified positive PyOM responders that increased in relative abundance belonging to the genera *Noviherbaspirillum*, *Pseudonocardia*, and *Gemmatimonas*. In contrast, fungal communities were less responsive to PyOM additions. Our findings expand our understanding of the post-fire cycling of PyOM and SOC, providing insights into the microbial mineralization of different PyOM-C fractions and their influence on soil C dynamics in fire-affected ecosystems.

1. Introduction

Since the mid-1970s, the number of forest wildfires in the western US and the percentage of area burned within them have increased due to a warming climate (Westerling, 2016). Increasing fire frequencies can have a negative impact on carbon (C) storage in forest soils, predominantly due to combustion of wood and litter as well as organic matter in the upper soil layers, leading to direct C losses from the system (Pellegrini et al., 2018). Simultaneously, fires can have an indirect positive impact on C storage via the production of pyrogenic organic matter (PyOM) (Santín et al., 2015). For example, during fires in pine-dominated forest systems, between 5 and 27 % of the biomass C can be converted to PyOM, which is likely to persist in soils due to a high proportion of C that is resistant to degradation (DeLuca et al., 2020;

Santín et al., 2015). In addition to natural production during wildfires, biochar is PyOM that is intentionally produced for use as a soil amendment and for C management strategy (Lehmann and Joseph, 2012). The conditions under which the addition of PyOM/biochar to soils will have a net positive C impact is still not clearly understood and depends on many factors, including the chemical composition and mineralizability of PyOM itself and whether its presence in soil affects the mineralizability of soil organic carbon (SOC) (Maestrini et al., 2015; Wang et al., 2016; Whitman et al., 2015). A key step to addressing this problem is taking a mechanistic approach to understanding how soil microbes decompose different carbon fractions of PyOM in fire-affected soils. This is the overarching goal of this study.

In recent years, through a combination of field studies and lab incubations, we have gained a better understanding of the factors that

* Corresponding author.

E-mail address: nayelazeba@berkeley.edu (N. Zeba).

¹ Present address: Department of Environmental Science, Policy, and Management, University of California, Berkeley, 2151 Berkeley Way, Berkeley, CA, 94704, USA.

affect the mineralization of PyOM by soil microbes. These factors primarily include PyOM chemical and physical properties, soil characteristics, and the duration of measurement (Wang et al., 2016; Zeba et al., 2022). These same factors also determine whether PyOM additions will alter the mineralization of the native SOC – i.e., whether PyOM addition will induce a *priming* effect (DeCuiques et al., 2018; Maestrini et al., 2015; Wang et al., 2016; Whitman et al., 2015). Among the mechanisms proposed to explain these priming effects, C heterogeneity in PyOM emerges as an important factor. For instance, *co-metabolism* is cited as a key mechanism for increased SOC mineralization after PyOM addition (positive priming) and is attributed to a small fraction of PyOM-C being easily mineralizable by microbes leading to increased microbial activity and subsequent mineralization of SOC (Hamer et al., 2004; Keith et al., 2011; Santos et al., 2012; Whitman et al., 2014a). Conversely, the availability of easily mineralizable C might reduce SOC mineralization (negative priming) via *substrate switching* when microbes preferentially use PyOM-C instead of SOC. Another explanation for negative priming often cited is the sorption of SOC to PyOM (Maestrini et al., 2015; Whitman et al., 2015), which would be expected to be associated with the more persistent PyOM-C fractions. This highlights that a key challenge to making these predictions is that PyOM is not homogeneous, even within a given sample, and that different PyOM fractions may play fundamentally different roles in determining its net effect on soil C stocks. To date, a persistent challenge has been to clearly differentiate between the different PyOM-C fractions and independently trace the fate and impact of these different PyOM fractions. Challenges include the fact that adding them to soil separately would undermine the objective of understanding how these fractions cycle in the context of bulk PyOM additions. Additionally, extensive, time-intensive sampling is necessary to track how the various C sources in the system react post-PyOM additions as mineralization of PyOM-C can occur rapidly in the first few days upon addition (Keith et al., 2011).

The nature of PyOM-C fractions also plays an important role in how PyOM additions affect soil microbes in the short term (Whitman et al., 2014a). A relatively small number of lab and field studies (summarized in Woolet and Whitman, 2020), have often found significant effects of PyOM on soil bacterial community composition, although soil characteristics played a more important role than PyOM in predicting community composition across soil types (Woolet and Whitman, 2020). In addition to community-wide effects, certain PyOM-responsive genera have been found to have a consistently positive response to PyOM across soil types – these genera include known fire responders, and many have members that are known polycyclic aromatic hydrocarbon (PAH) degraders, indicating a potential capacity to break down complex aromatic C fractions in PyOM (Woolet and Whitman, 2020). Besides PyOM-responsive taxa identified via high throughput sequencing, specific bacteria (e.g., *Streptomyces* sp.) readily grow on agar media containing PyOM-C as the sole carbon source (Zeba et al., 2022), while others (e.g., *Pseudomonas* sp. and taxa from the family *Pseudonocardiaceae*) can colonize the PyOM surface (Dai et al., 2017; Tu et al., 2020).

For fungi, much of our understanding of the effects of PyOM comes from studying fungal responses to fire. Certain fungi, such as *Pholiota*, *Pyronema* and *Penicillium* sp. are known to thrive in post-fire environments (Fox et al., 2022). Their potential to exploit post-fire resources, such as PyOM, could contribute to their relative increase (Enright et al., 2022; Fischer et al., 2021; Whitman et al., 2019), along with other factors like heat tolerance (Bruns et al., 2020; Fox et al., 2022). A few studies examining the effects of PyOM application on fungi have observed changes in the fungal community structure, primarily driven by alterations in soil properties (Gao et al., 2021; Yao et al., 2017). The aromatic C fraction in PyOM may also play an important role in shaping the fungal community composition (Li et al., 2019). For instance, dominant post-fire fungus, *Pyronema domesticum* has the capacity to break down complex aromatic C when grown on agar media containing PyOM-C (Fischer et al., 2021).

While the list of PyOM-responsive fungal and bacterial taxa is

growing, the mechanisms by which both the community and individual taxa respond to PyOM are poorly understood. Specifically, with regard to the C heterogeneity of PyOM, it is likely that the relative abundance of some species increases in response to the easily mineralizable PyOM-C fractions, while others increase in response to the more aromatic PyOM-C fractions. Although methods like stable isotope probing would be required to conclusively demonstrate these different responses, such differential responses to different fractions should result in a time-dependent response even during a short-term incubation study – i.e., we would expect responders to the easily mineralizable PyOM-C fraction to increase early in the incubation period, as this fraction is consumed early on, while responders to the aromatic C fractions should emerge later.

In this study, we partitioned the C in PyOM into two fractions – the water extractable fraction (representing the easily mineralizable fraction) and the non-water-extractable fraction (representing the more persistent, water-insoluble fraction). Firstly, we aimed to determine the extent to which the two C fractions within bulk PyOM are differentially mineralized by microbes and how this affects the mineralization of SOC. Secondly, we aimed to track shifts in microbial community composition and identify PyOM-responsive taxa during the incubation period.

For the first objective, we sought to isolate the short-term dynamics of the water-extractable vs. non-water-extractable PyOM fraction, given that positive priming effects usually occur over relatively short time-scales. We addressed this by tracking the mineralization of ^{13}C labeled water-extractable and ^{13}C labeled non-water-extractable PyOM-C in soil-PyOM incubations and used this information to decipher the dominant priming mechanisms. We hypothesized that the water-extractable PyOM-C fraction would be more rapidly mineralized, since it primarily consists of aliphatic C compounds that are readily consumed by microbes, and that the mineralizability of this fraction would be a strong predictor of SOC priming. We also predicted that differences in the relative abundance of this easily mineralizable fraction would be reflected in the degree to which PyOM stimulates microbial activity, thereby increasing the rate of SOC mineralization (i.e., inducing a positive priming effect via co-metabolism) in the short term (Maestrini et al., 2015; Whitman et al., 2014b).

For the second objective, our aim was to identify microbial responders that increase in relative abundance during periods of high vs. low water-extractable PyOM-C mineralization. To address this, we conducted a parallel set of soil-PyOM incubations to track shifts in microbial community composition and identify PyOM-responsive taxa at key time points, informed by real-time isotopically partitioned PyOM-C mineralization data. This enabled us to differentiate between early (water-extractable PyOM-responders) vs. late (non-water-extractable PyOM-responders) taxa. Additionally, we used LC-MS analysis to track changes in the soil chemical profile during these select time points to characterize the nature of carbon compounds available to soil microbes during the incubation. We hypothesized that PyOM addition would result in shifts in both the bacterial and fungal communities within the first few days, tracking with the consumption of the easily mineralizable water-extractable fraction. We expected PyOM responders to belong to known fire-responsive and PyOM-responsive genera. We predicted that early responders would mostly be bacteria, while late responders could include both bacteria and fungi that have the ability to degrade complex aromatic C structures, such as *Rhodococcus*, *Sphingomonas* and *Pyronema* sp. (Fischer et al., 2021; Ghosal et al., 2016).

2. Materials and methods

2.1. Soil description

To increase the likelihood of finding PyOM-adapted taxa, we targeted a soil with known burn history. Soil was collected in the winter of 2020 from the El Dorado National Forest in California from a region that burned during the 2014 King Fire (38.86953, -120.61322). The soil

belongs to the Pilliken series and is a Coarse-loamy, mixed, mesic Entic Xerumbrept. Topsoil (0–10 cm) was collected from six sampling spots within a 10 m² area after removing the O-horizon and litter layer. These samples were initially stored at –20 °C and were then shipped to Madison, WI on dry ice. Upon arrival, the replicate soil samples were homogenized, combined into a single composite sample, and stored at –20 °C until the start of the incubation. These soils naturally freeze, so we expect that the freezing process would not have completely unrealistic effects on the microbial community composition. We chose to focus on the top 10 cm of mineral soil as this horizon would be expected to have meaningful contact with surface produced PyOM after a wildfire. Standard soil properties (Table 1) were analyzed at the UW Soil and Forage Lab with a sample that was thawed and sieved to < 2 mm.

2.2. Biomass production

Two-year-old eastern white pine tree seedlings (*Pinus strobus* (L.)) from the Wisconsin Department of Natural Resources (DNR) were grown in an enriched ¹³CO₂ atmosphere custom growth chamber for one growing season. The trees were pulse labeled with 99 % ¹³CO₂ at regular intervals over the course of their growth with the goal of producing evenly labeled trees. The labeled trees were watered with deionized water and Hoagland's solution (Supplemental Note S1).

A paired same-aged set of eastern white pine trees from the Wisconsin DNR, grown under ambient, non-enriched CO₂, was used as an unlabeled control for this study, keeping moisture, humidity, and light conditions equivalent. (Labeled and unlabeled biomass properties are provided in Table S1).

2.3. PyOM production and analyses

We used the aboveground biomass of the eastern white pine trees to produce PyOM. For each set of labeled and unlabeled trees, we ground tree stems and needles and mixed them in a 1:4 ratio to account for any chemical differences between needles and stems. We pyrolyzed both sets of trees at 350 °C (referred to as “Py350”) and 550 °C (referred to as “Py550”) in a modified Fischer Scientific Lindberg/Blue M Moldatherm box furnace (Thermo Fisher Scientific, Waltham, MA, United States) fitted with an Omega CN9600 SERIES Autotune Temperature Controller (Omega Engineering Inc., Norwalk, CT, United States). The PyOM was ground using a mortar and pestle and sieved to collect PyOM with particle size <45 μm. (Additional details in Supplemental Note S2).

Total C, nitrogen (N) and bulk δ¹³C were measured at the Cornell Stable Isotope Laboratory (COIL) using a Delta V Isotope Ratio Mass Spectrometer (Thermo Fisher Scientific) interfaced to a dry combustion Carlo Erba NC2500 Elemental Analyzer (Carlo Erba Instruments, Milan, Italy). Total hydrogen (H) and oxygen (O) were also measured at COIL on a Delta V Isotope Ratio Mass Spectrometer interfaced to a Temperature Conversion Elemental Analyzer (Thermo Fisher Scientific). The pH

was measured in deionized water at a 1:20 solid:solution ratio using an Inlab Micro Combination pH electrode (Mettler Toledo, Columbus, OH, United States) connected to a Thermo Scientific Orion Star A111 benchtop pH meter (Thermo Fisher Scientific). The properties of all PyOM materials are provided in Table 2.

2.4. Water-extractable PyOM-C extraction and exchange

To isolate and compare the mineralization rates between water-extractable and non-water-extractable PyOM-C fractions, we removed and exchanged the water-extractable fraction from the ¹³C labeled vs. unlabeled PyOM, at C-equivalent rates. This resulted in two PyOM treatments (Fig. 1): ¹³C water-extractable PyOM (where the water-extractable fraction was ¹³C-labeled) and ¹³C non-water-extractable PyOM (where the non-water-extractable fraction was ¹³C-labeled). As controls, we extracted and then returned (remixed) the water-extractable fractions for the ¹³C PyOM and unlabeled PyOM samples at the same rates. After exchange, samples were pH-adjusted to match that of soil and dried before use in the incubation study in order to control for pH effects and isolate C-related phenomena. (Additional details in Supplemental Note S3).

Before returning the water-extractable fraction (DOC) to the non-water-extractable PyOM, we dried the non-water-extractable PyOM at 70 °C and measured total C, N, bulk δ¹³C and pH as described above. We also measured the total organic carbon (TOC) content of the non-water-extractable PyOM, at the UW Soil and Forage Lab using the dry combustion technique (Table S2). The ratios of water-extractable to non-water-extractable PyOM-C were selected to match the DOC content of the water-extracted PyOM for the ¹³C labeled Py350 and Py550 treatments (Table 2). Thus, all Py350 treatments had 2.1 mg water-extractable PyOM-C g⁻¹ non-water-extractable PyOM-C, while all Py550 treatments had 1 mg water-extractable PyOM-C g⁻¹ non-water-extractable PyOM-C.

2.5. Incubation setup and monitoring

Before the incubation, soil was thawed, sieved to <2 mm and maintained at room temperature and open to the air for two weeks. We used a sub-sample of the soil to determine field capacity for unamended and PyOM-amended soils (Py350 and Py550) separately to ensure equivalent moisture levels with and without PyOM additions. Water holding capacity was determined as in Whitman et al. (2021). The moisture content of the thawed soils was determined one day before the start of the incubation to calculate the water required to reach target moisture levels of 65 % field capacity for each treatment.

We ran two sets of parallel incubations – (i) a CO₂ flux monitoring

Table 2
Properties of PyOM.^a

Property (units)	¹³ C labeled		Unlabeled	
	350 °C	550 °C	350 °C	550 °C
pH (H ₂ O)	9.42	10.09	7.97	10.19
Total C (%)	64.75 ± 2.64	71.87 ± 1.35	72.87 ± 8.43	78.17 ± 1.81
Total N (%)	3.24 ± 0.15	2.91 ± 0.05	2.82 ± 0.31	2.47 ± 0.06
Total H (%)	3.52	1.75	3.78	1.93
Total O (%)	16.28	10.96	17.46	9.32
Bulk δ ¹³ C vs. VPDB (‰)	1513.12 ± 9.47	1596.51 ± 8.32	–29.38 ± 0.05	–29.27 ± 0.08
Total water extractable C (DOC) (mg g ⁻¹ PyOM)	2.11	0.95	1.24	0.67

^a pH values of the original PyOM before adjustment are shown. The values presented for total C, total N and bulk δ¹³C are means of five replicates ± standard deviation. The values for total water-extractable C represent DOC in original PyOM before exchange.

Table 1
Properties of soil collected from the 2014 King fire affected region.^a

Property (units)	
Sand (%)	55
Silt (%)	24
Clay (%)	20
Texture (USDA classification)	Sandy clay loam
Total C (%)	7.79
Total N (%)	0.46
Bulk δ ¹³ C vs. VPDB (‰)	–27.07
NO ₃ -N (ppm)	28.8
NH ₄ -N (ppm)	4.9
Available P (ppm)	9
Available K (ppm)	84
pH (H ₂ O)	6.1

^a The values represent a single measurement of homogenized soil mix from six replicate sampling spots.

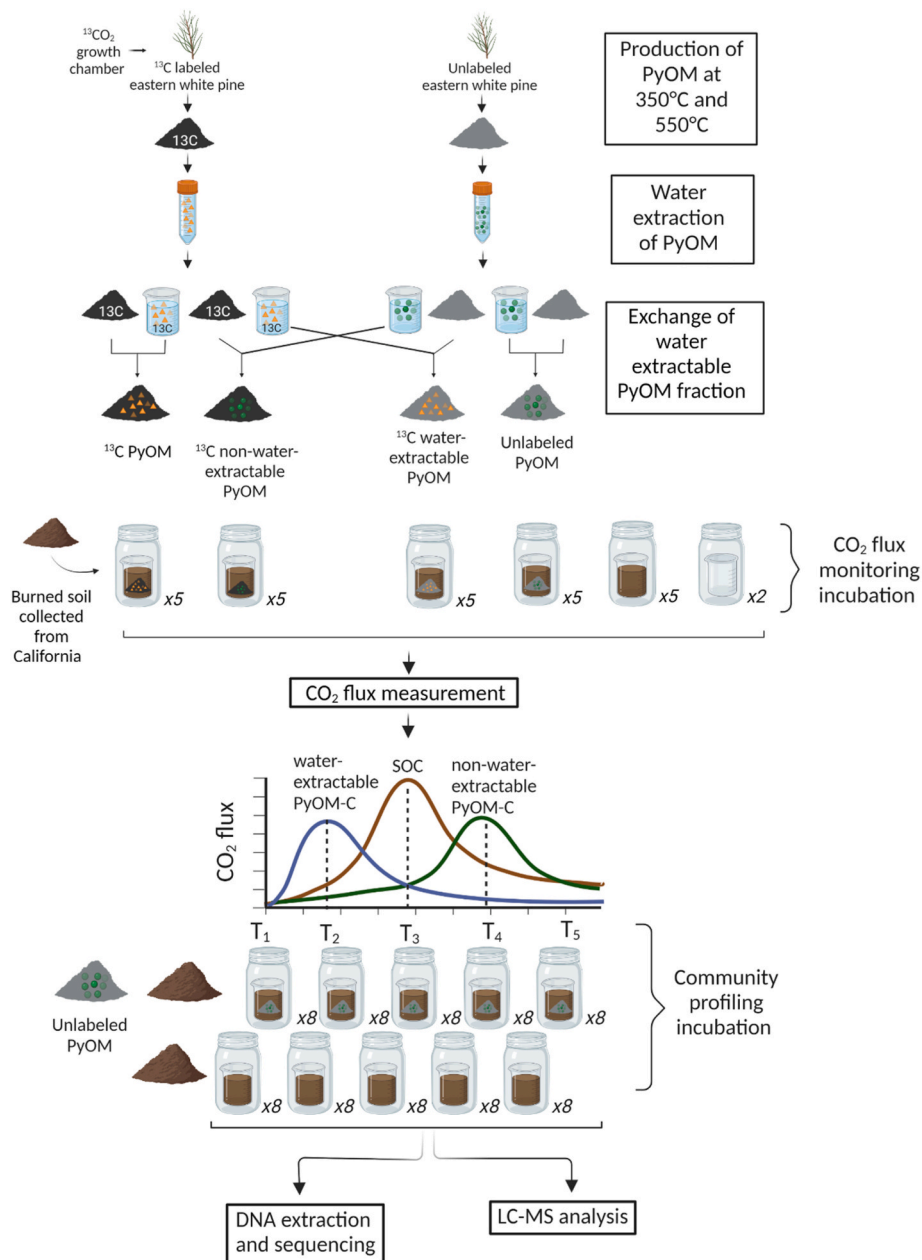


Fig. 1. Experimental setup. Production, extraction and exchange of PyOM followed by incubation set up and monitoring. The number of replicate incubations for each treatment/timepoint have been indicated by 'x' next to the jar.

incubation to partition C mineralization between different PyOM fractions and (ii) a community profiling incubation to analyze the effects of PyOM on microbial community composition at critical time points during the incubation. We analyzed data from the CO_2 flux monitoring incubation in real time, so we could dynamically select 4–5 timepoints for community profiling that reflect initial conditions, peak PyOM-C mineralization, peak SOC mineralization and final conditions. At each of these selected timepoints, sample jars from the community profiling incubation were frozen for DNA sequencing. For the flux monitoring jars, we had five replicates for each PyOM temperature and each treatment (Fig. 1): (i) Soil + unlabeled PyOM (ii) Soil + ^{13}C PyOM (iii) Soil + ^{13}C water-extractable PyOM (iv) Soil + ^{13}C non-water-extractable PyOM (v) Unamended soil control. For the parallel community sequencing jars, we had eight replicates destructively sampled at each timepoint, with the following treatments (Fig. 1): (i) Soil + unlabeled PyOM (the same treatment that was used for the flux monitoring incubation) (ii)

Unamended soil control.

Incubations were performed in 60 mL glass jars placed inside pint-sized Mason jars (473 mL). Each 60 mL glass jar received 3.5 g soil on a dry mass basis and the PyOM-amended jars received PyOM at a consistent rate of 18 mg TOC PyOM g^{-1} dry soil (*i.e.*, 3.1 % dry mass addition for Py350 and 2.8 % dry mass addition for Py550). These addition rates were designed to represent locally high inputs of PyOM after a wildfire (Reisser et al., 2016). We added water dropwise to gradually bring up the moisture of each jar to the target moisture level of 65 % field capacity.

2.5.1. CO_2 flux monitoring incubation

After moisture adjustment, we placed the 60 mL glass jars inside Mason jars containing 20 mL acidified deionized water (pH ~4) at the bottom to maintain humidity and prevent water loss. Acidified water was specifically used during the CO_2 flux monitoring incubation to

reduce potential dissolution of CO₂ or release of any carbonates in the water into the incubation atmosphere, which could lead to inaccuracies in our data. We capped and sealed the jars with sterile, gas-tight lids with fittings for CO₂ gas measurements and connected them to randomly selected positions on the distribution manifolds (multiplexer) using polyurethane tubing (Berry et al., 2021). The connected jars were immediately flushed with a 400 ppm CO₂-air gas mixture to reset the headspace CO₂ concentration in all jars at the initial timepoint. We incubated the jars at room temperature in the dark and measured the concentration of CO₂ emitted in the headspace of each jar at frequent intervals using a Picarro G2131i cavity ringdown spectrometer (Picarro Inc., Santa Clara, CA, United States) attached to the multiplexer over a period of one month. For Py350, we measured headspace CO₂ concentration at intervals of 6 h during the first 2 days, and gradually increased the intervals to 12 h during the first and second weeks, 24 h during the third week and 48 h during the last week of incubation. Similarly, for Py550, we measured headspace CO₂ concentration every 6–12 h during the first 3 days, 24 h during the first and second weeks and 48–72 h till the end of the incubation. After each measurement, we flushed the jars with the 400 ppm CO₂-air gas mixture to prevent oxygen depletion and excessive CO₂ accumulation inside the jars. The precise concentration after flushing each jar was measured and subtracted from the next timepoint reading to calculate the emitted CO₂ in the jar during that interval.

2.5.2. Community profiling incubation

For community profiling, after moisture adjustment, we placed the glass jars inside Mason jars containing 20 mL deionized water at the bottom and capped them with sterile regular lids. The jars were then incubated in the dark at room temperature. During the incubation, the jars were opened for 1–2 min every 48 h to prevent oxygen depletion inside the Mason jars and to mirror the CO₂ flux incubations. We checked the mass of the jars once a week to determine moisture loss and water was added to return jars to target moisture levels. At each sampling timepoint, eight jars were destructively sampled and placed in sterile Whirl-Pak bags (Nasco, Fort Atkinson, WI, United States) and stored at –80 °C until DNA extraction was performed. During the setup, eight unamended and PyOM-amended soil samples were randomly selected and frozen to represent community profile on Day 0.

2.6. ¹³CO₂ partitioning and statistical analyses

We used R Studio (v4.2.2) (R Core Team, 2022) with the ‘tidyverse’ (Wickham et al., 2019), ‘zoo’ (Zeileis and Grothendieck, 2005) and ‘broom’ (Robinson et al., 2022) packages to process raw CO₂ readings from the multiplexer-Picarro system. Stable isotope partitioning, as represented by Equation (1), was used to partition the CO₂ emissions from the flux monitoring treatments to determine the fraction of CO₂ emitted from water-extractable PyOM, non-water-extractable PyOM, and soil in the PyOM-amended incubations.

$$f_A = (\delta_{Total} - \delta_B) / (\delta_A - \delta_B) \quad (1)$$

Equation (1) calculates the fraction of CO₂ emitted from source A (f_A) using the ¹³C isotopic composition of the total respired CO₂ (δ_{Total}), CO₂ respired from source A (δ_A), and source B (δ_B).

For example, we partitioned the total CO₂ emissions from the “Soil + ¹³C water-extractable PyOM” treatments into two sources: CO₂ emitted from the ¹³C labeled water-extractable PyOM source and CO₂ emitted from the unlabeled soil and non-water-extractable PyOM source. We calculated the fraction of total CO₂ emitted from the water-extractable PyOM source ($f_{water-extractable\ PyOM}$) using Equation (2):

$$f_{water-extractable\ PyOM} = (\delta_{Total\ CO_2} - \delta_{CO_2\ soil + non-water-extractable\ PyOM}) / (\delta_{CO_2\ water-extractable\ PyOM} - \delta_{CO_2\ soil + non-water-extractable\ PyOM}) \quad (2)$$

In this equation,

$\delta_{Total\ CO_2}$ represents the mean isotopic composition of the total CO₂ emitted from the “Soil + ¹³C water-extractable PyOM” treatments, $\delta_{CO_2\ soil + non-water-extractable\ PyOM}$ represents the mean isotopic composition of the CO₂ emitted from soil and non-water-extractable PyOM (determined from the “Soil + unlabeled PyOM” treatments), and $\delta_{CO_2\ water-extractable\ PyOM}$ represents the isotopic composition of the CO₂ emitted from water-extractable PyOM, assumed to be the isotopic composition of the ¹³C labeled PyOM.

Similarly, we determined the fraction of CO₂ emitted from non-water-extractable PyOM ($f_{non-water-extractable\ PyOM}$) and the fraction of CO₂ emitted from SOC (f_{SOC}) by partitioning the flux from other treatments (Supplemental Note S4). We note that the isotopic composition of the labeled water-extractable and non-water-extractable PyOM-C fractions may differ slightly; however, small differences in isotopic composition of the bulk ¹³C-labeled PyOM for CO₂ emitted from both fractions would not meaningfully impact our overall partitioning results (Fig. S1).

To assess the extent to which the two C fractions within bulk PyOM are differentially mineralized by microbes, we determined the mineralizability of the PyOM-C fractions by normalizing the amount of C mineralized to the quantity of each C fraction added to the jars. We also determined the mineralizability of the SOC for comparison. Prior to statistical analysis, we assessed the normality and homogeneity of variance across treatment groups using the Shapiro and Bartlett test functions in the R ‘stats’ package. To test for significant differences in mineralizability between the PyOM-C fractions and SOC, given unequal variances, we used Welch’s ANOVA and the Games-Howell post-hoc tests using the ‘rstatix’ package (Kassambara, 2022).

To identify the priming effect of PyOM on SOC, we quantified priming as:

$$\text{Priming of SOC} = [\text{SOC}_{(\text{PyOM-amended})} - \text{SOC}_{(\text{unamended})}] / \text{SOC}_{(\text{unamended})}$$

where $\text{SOC}_{(\text{PyOM-amended})}$ represents the rate or cumulative SOC mineralization in presence of PyOM and $\text{SOC}_{(\text{unamended})}$ indicates the rate or cumulative SOC mineralization in absence of PyOM.

All code used for flux partitioning, data analyses and figures in this manuscript is available at <https://github.com/nayelazeba/Chapter3>.

2.7. Microbial community analyses

2.7.1. DNA extraction, amplification, and sequencing

We extracted DNA from each soil sample using the DNEasy PowerLyzer PowerSoil DNA extraction kit (QIAGEN, Hilden, Germany), following the manufacturer’s instructions. One blank extraction without soil was included for every 24 samples. We performed PCR in triplicate to amplify the extracted DNA, targeting the 16S rRNA gene v4 region in bacteria and archaea with 515f and 806r primers (Walters et al., 2015), and targeting the ITS2 gene region in fungi with 5.8S-Fun and ITS4-Fun primers (Taylor et al., 2016) with barcodes and Illumina sequencing adapters added as per Kozich et al. (2013). During PCR, we included one negative control (PCR-grade water) and one positive control (known microbial community mix) for every 30 samples. The PCR amplicon triplicates were pooled, purified and normalized using a SequalPrep Normalization Plate (96) Kit (Thermo Fisher Scientific). Samples, including blanks, were pooled and library cleanup was performed using a Wizard SV Gel and PCR Clean-Up System A9282 (Promega Corporation, Madison, United States) according to manufacturer’s instructions. A detailed procedure for the DNA extraction and PCR amplification and purification is described in Whitman et al. (2019). We submitted the pooled library to the UW Madison Biotechnology Center for 2 x 300 paired end Illumina MiSeq sequencing (Illumina Inc., San Diego, CA, United States) for both 16S and ITS2 amplicons.

2.7.2. Sequence data processing and taxonomic assignments

We used the QIIME2 pipeline (QIIME2, v2020.6 (Bolyen et al.,

2019)) to process the sequences following the steps described in [Woollet and Whitman \(2020\)](#). The sequence processing steps were performed on the UW-Madison Centre for High Throughput Computing cluster. Raw sequence data were demultiplexed and quality filtered followed by denoising with DADA2 ([Callahan et al., 2016](#)). The DADA2 denoise-paired command as implemented within QIIME2 was used to determine operational taxonomic units (OTUs). This resulted in a retention of a mean of 45,246 16S sequences and a mean of 27,358 ITS2 sequences per sample. For ITS2 reads, we then ran the sequences through ITSx ([Bengtsson-Palme et al., 2013](#)) to identify fungi and to remove plant and other eukaryotic sequences. Taxonomy was assigned to the 16S sequences using the Silva 138 database ([Quast et al., 2013](#)) at 99 % similarity using the QIIME2 feature-classifier classify-sklearn. Pre-trained taxonomy classifiers specific to the primers used for 16S sequencing were used ([Bokulich et al., 2018](#)). For the IT2 reads, we assigned taxonomy using the UNITE 'developer' database (v8.3) at 99 % similarity ([Abarenkov et al., 2021](#)). UNITE taxonomy classifiers were trained on the full reference sequences using the QIIME2 feature-classifier fit-classifier-naive-bayes ([Pedregosa et al., 2011](#)).

2.7.3. Statistical analyses

We worked in R Studio, primarily with the 'phyloseq' ([McMurdie and Holmes, 2013](#)) and 'vegan' packages ([Oksanen et al., 2022](#)), to compare microbial community composition between unamended soil and PyOM-amended soil samples. We removed 381 OTUs that belonged to "Chloroplast" and "Mitochondria" in the 16S OTU table and removed samples with less than 6650 16S reads and 1560 ITS2 reads. We then calculated Bray-Curtis dissimilarity between samples ([Bray and Curtis, 1957](#)), normalized by relative abundance and represented them as NMDS ordinations. We tested for significant effects of PyOM addition after controlling for time using permutational multivariate ANOVA (PERMANOVA) on Bray-Curtis dissimilarities, implemented in vegan as the 'adonis2' function.

To identify PyOM-responsive taxa, we calculated log₂-fold changes in taxon abundances in unamended vs. PyOM-amended soils using the 'DESeq2' R package, which is used to analyze differential abundance between treatments ([Love et al., 2014](#)). To test for specific effects of PyOM addition on taxon abundance, we used a design formula that models differences in taxon abundance across samples on Day 0, over time and due to PyOM addition over time ([Love et al., 2016](#), p. 201). We then performed a likelihood ratio test with a reduced model without the PyOM addition effects over time to identify significant responder OTUs (Benjamini and Hochberg correction, adjusted p value < 0.05). This approach allowed us to identify only those taxa that at one or more time points after Day 0 showed a significant log₂-fold change with PyOM addition.

The *t*-test function from the 'stats' R package was used to test for significant differences in relative abundances between PyOM-amended and unamended soils for PyOM-responsive genera identified using DESeq2.

2.8. LC-MS analysis

To acquire chemical profiles, we first prepared chemical extracts by combining 0.4 g of soil with 4 mL of LC/MS-grade methanol, sonicated for 5 min, and then shook them overnight (~16 h) at 25 °C and 200 rpm. Blank extraction controls were prepared in parallel, in which empty tubes lacking any soil sample were subjected to the same chemical extraction protocol. Solids were allowed to settle to the bottom for 30 min and then 3.5 mL was carefully collected from the top and immediately dried via a Savant SPD1010 SpeedVac Concentrator (Thermo Fisher Scientific). To analyze these dried extracts via LC/MS, we resuspended them in 1 mL of 100 nM nonactin LC/MS-grade methanol solution, to a final concentration of approximately 1 mg extract/1 mL of solvent. These resuspended samples were sonicated for 5 min to ensure that the extract dissolved into the solvent, and then centrifuged at

15,000 rpm to pellet any particulate, after which, 900 µL of solution was transferred to an HPLC vial. To create a pooled quality control (QC) sample we combined 10 µL of each sample. Samples were analyzed in a randomized order with a methanol blank and pooled QC analyzed after every 12 samples. Samples were analyzed with an ultra-high-pressure liquid chromatography (UHPLC) system Dionex Ultimate 3000 (Thermo Fisher Scientific) coupled to a high-resolution mass spectrometer (HRMS) Thermo Q-Exactive Quadrupole-Orbitrap (Thermo Fisher Scientific) using a heated electrospray ionization (HESI) source and a C18 column (Thermo Scientific Acclaim rapid-separation liquid chromatography [RSLC] system, 50 mm by 2.1 mm, 2.2 µm pore size). We used the following 20 min UHPLC method; 1 min 40 % acetonitrile (ACN) plus 0.1 % formic acid (FA), 1 min gradient from 40 % to 65 % ACN plus 0.1 % FA, 11 min gradient from 65 % to 99 % ACN plus 0.1 % FA, 3.5 min 99 % ACN plus 0.1 % FA, 0.5 min gradient from 99 % to 40 % ACN plus 0.1 % FA, and 3 min re-equilibration in 40 % ACN plus 0.1 % FA; injection volume of 5 µL, flow rate of 0.4 mL/min, and column oven temperature of 35 °C. The full MS1 scan was performed in positive mode at a resolution of 35,000 FWHM (full width at half-maximum) with an automatic gain control (AGC) target of 1e6 ions and a maximum ion injection time (IT) of 100 ms with a mass range from m/z 200 to m/z 2000. Data were processed using MS-DIAL v4.9 ([Tsugawa et al., 2015](#)). We used R v4.1.3 to omit features with a peak height value greater than 100,000 in any negative control samples (*i.e.*, methanol blanks and blank extraction controls) prior to ordination and statistical analyses as described above.

3. Results

3.1. PyOM-C and SOC flux dynamics

Over the 30-day incubation, the mineralizability of PyOM-C from the water-extractable fraction was significantly higher than that of the non-water-extractable PyOM-C fraction and soil organic carbon for both the Py350 and Py550 treatments ($p < 0.05$, Games-Howell post-hoc test; [Fig. 2A](#)). The amount of C mineralized per gram of initial C from the water-extractable fraction was 10 and 50 times higher than the non-water-extractable PyOM-C in the Py350 and Py550 treatments, respectively. The C mineralizability of the Py350 non-water-extractable PyOM-C fraction was higher than that of soil organic carbon. However, this pattern was not observed in the Py550 treatment, where the C mineralizability of soil organic carbon was higher. Our focus in this study was to compare the relative mineralizability of the different PyOM-C fractions with soil organic carbon (*i.e.*, on a per carbon gram basis). If we consider the total C mineralized, the cumulative mineralization from the water-extractable PyOM-C fractions was lower compared to the non-water-extractable PyOM-C and SOC, as would be expected due to the small fraction of total PyOM represented by water-extractable PyOM-C in the jars ([Fig. S2](#)).

The addition of Py350 resulted in a net 57 % increase in cumulative SOC mineralization after 30 days of incubation, indicating a strong positive priming effect ([Fig. 2B](#)). This effect was immediately apparent, with cumulative SOC mineralization in the Py350-amended soils being over 100 % higher than in the unamended soils after just 5 days of incubation. However, this strong positive priming effect diminished after 5 days, although the net effect remained positive for the duration of the study. In contrast, the addition of Py550 resulted in a net 17 % decrease in cumulative SOC mineralization, indicating a negative priming effect. This negative priming was also observed immediately upon the start of the incubation, with the cumulative amount of SOC mineralized in the Py550-amended soils being on average 8 % lower than in the unamended soil treatments during the first 10 days of incubation.

3.2. Microbial community composition and PyOM positive responders

We observed significant shifts in the bacterial and archaeal

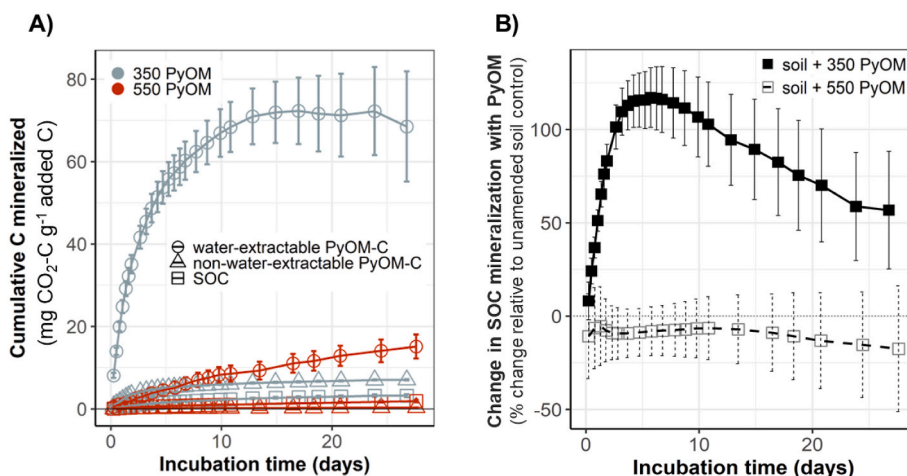


Fig. 2. A) Mineralizability of PyOM fractions and SOC over time. Cumulative mean C mineralized per gram of added C for water-extractable PyOM-C, non-water-extractable PyOM-C and SOC. (n = 4–5, error bars = SE). **B) Effect of PyOM addition on SOC mineralizability.** Cumulative mean SOC priming over time represented as % change in SOC mineralization in PyOM-amended soils relative to the control unamended soils. Priming calculated as: $[\text{SOC}_{(\text{PyOM-amended})} - \text{SOC}_{(\text{unamended})}] / \text{SOC}_{(\text{unamended})}$ (n = 4–5, error bars = SE).

community composition over time (PERMANOVA, $p_{\text{time}} = 0.001$) and in response to the addition of Py350 (PERMANOVA, $p_{\text{Py350}} = 0.005$, $R^2_{\text{Py350}} = 0.03$, Fig. 3A) and Py550 (PERMANOVA, $p_{\text{Py550}} = 0.005$, $R^2_{\text{Py550}} = 0.04$, Fig. 3C) after controlling for time. The impact of PyOM was evident within a few days of incubation – the communities in both the Py350 and Py550-amended soils were distinct from the unamended soils by Day 2 and Day 4, respectively. In contrast, we only detected significant shifts in the fungal community composition over time (PERMANOVA, $p_{\text{time}} < 0.01$ for both Py350 and Py550 treatments) and not in response to PyOM addition (Fig. 3B and 3D). Time had the most explanatory power for variations in both the bacterial and fungal

communities (R^2 values between 0.08 and 0.25).

Using DESeq2, we identified 19 bacterial OTUs (0.31 % of the total OTUs analyzed in DESeq2) that responded positively to the addition of Py350 (Fig. 4A). These OTUs showed a significant positive response to Py350 at one or more time points after Day 0 and had a mean normalized count higher than the 25th percentile. Among these responsive OTUs, 13 belonged to the following genera: *Bacillus*, *Massilia*, *Ferruginibacter*, *Gemmatimonas*, *Noviherbaspirillum*, *Pseudonocardia*, *Psychroglaciecola*, *Saccharimonadales*, and *Singulisphaera*. The remaining 6 OTUs were assigned to unknown genera. For *Gemmatimonas* and *Noviherbaspirillum*, we observed a significant increase in the relative abundance of all

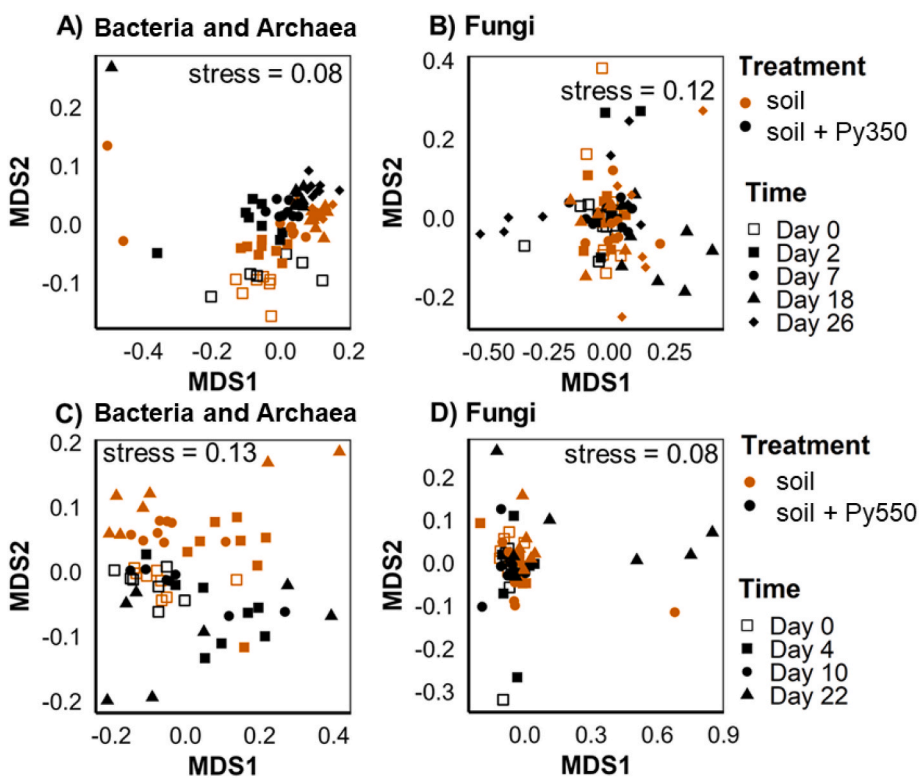


Fig. 3. Effect of PyOM addition on soil microbial community composition. NMDS ordination of Bray-Curtis dissimilarities between (A & C) bacterial/archaeal (16S rRNA gene v4 region) communities (k = 2) and (B & D) fungal (ITS2) communities (k = 3) for all samples. Top panels indicate data for Py350-amended and control unamended soil samples. Bottom panels indicate data for Py550-amended and control unamended soil samples.

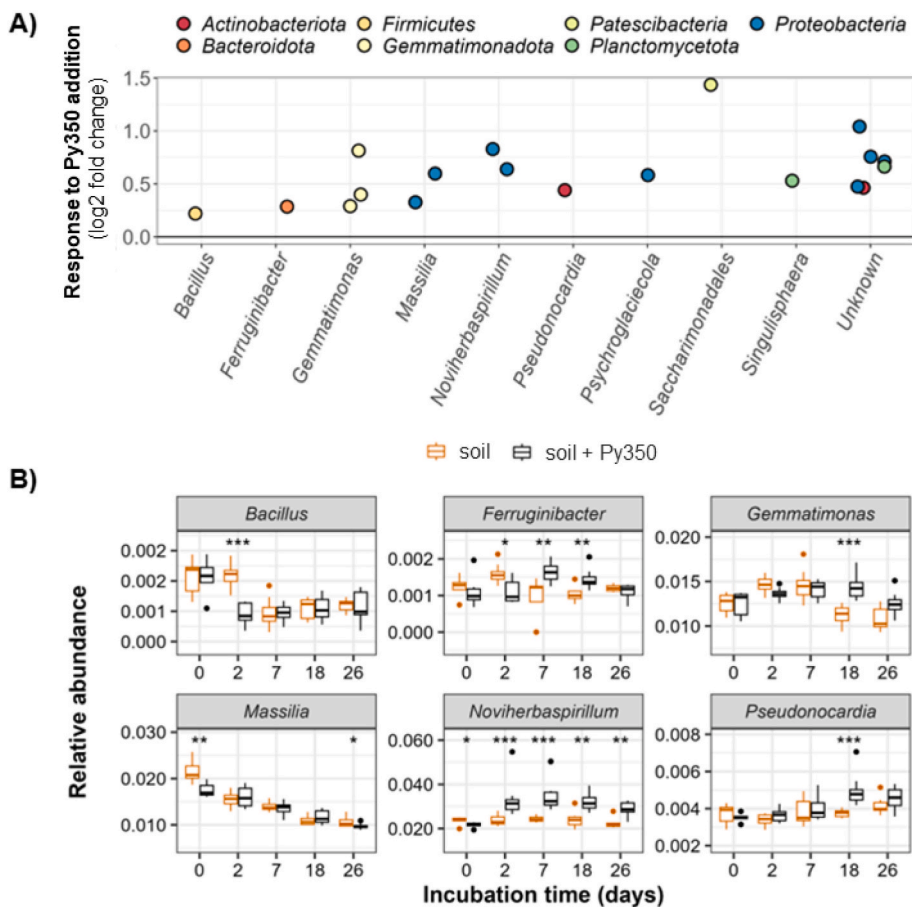


Fig. 4. Bacterial response to Py350. A) Log₂ fold change in in taxon abundance in Py350-amended vs. unamended soils, controlling for differences in taxon abundance across samples on Day 0 and over time. Each point represents a single 16S rRNA gene v4 region OTU with mean normalized count above the 25th percentile and that was significantly different in abundance in PyOM-amended vs. unamended soils (Benjamini and Hochberg correction, adjusted p value < 0.05). B) Relative abundance of six positive responsive genera over time (as identified using DESeq2) observed in the unamended and Py350-amended soils (n = 5–8). Data are grouped for multiple responder OTUs within a genus. * indicates relative abundances that differ significantly from unamended soil at a given timepoint (t-test, *: p < 0.05; **: p < 0.01; ***: p < 0.001).

responsive OTUs following the addition of Py350, with the increase appearing at different points during the incubation period (Fig. 4B). In the case of fungi, we identified 5 OTUs (0.26 % of the total OTUs analyzed in DESeq2) that showed a significant positive response to Py350 and had a mean normalized count higher than the 25th percentile

(Fig. S3). These OTUs belonged to the following genera: *Calyptrozyma*, *Coniochaeta*, *Holtermanniella*, *Leucosporidium* and *Solicoccozyma*. However, we did not observe an increase in relative abundance over time for any of the responsive fungal OTUs following the addition of Py350. Upon Py550 addition, we identified only a single bacterial OTU from the

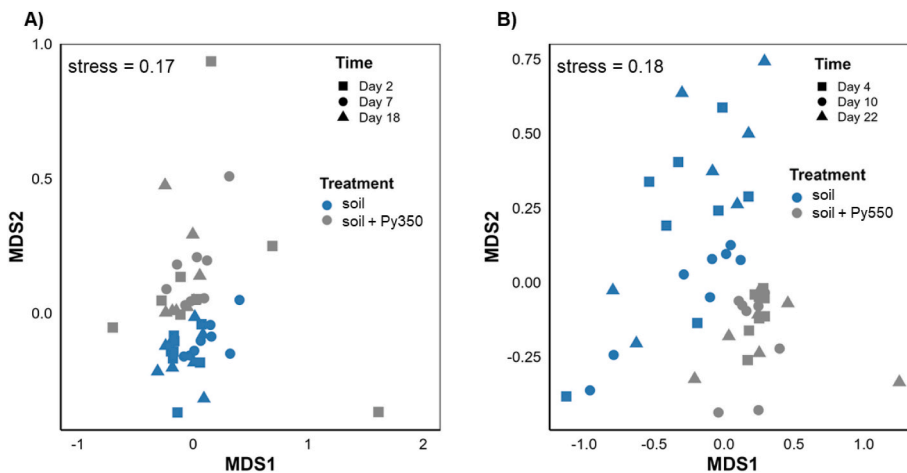


Fig. 5. Effect of PyOM addition on soil chemical profile. NMDS ordination of Bray-Curtis distances between soil chemical peaks for A) Py350-amended and control unamended soil samples (k = 2) and B) Py550-amended and control unamended soil samples (k = 2).

Gemmatimonas genus and a single fungal OTU from the *Paraphoma* genus that responded positively to its addition.

3.3. Effect of PyOM addition on soil chemical composition over time

The LC-MS analysis of methanol-extracted PyOM-amended and unamended soils showed that the addition of both Py350 and Py550 resulted in significant shifts in the soil chemical profile, after controlling for time (PERMANOVA, $p_{Py350} = 0.001$, $R^2_{Py350} = 0.05$; $p_{Py550} = 0.001$, $R^2_{Py550} = 0.06$; Fig. 5A and 5B).

4. Discussion

4.1. Mineralizability of PyOM differed between C fractions and with PyOM temperature

Consistent with our hypothesis, water-extractable C fractions in PyOM were much more readily mineralized than non-water-extractable C fractions (Fig. 2A). This 10-50x difference in C mineralizability underscores the heterogeneity of the C in PyOM and the potential to explain significant variation in PyOM decomposition rates. We calculated mineralization rates for the water-extractable PyOM-C fractions of 0.23 % day⁻¹ for Py350 and 0.04 % day⁻¹ for Py550. These rates surpass decomposition rates estimated by the meta-analysis of Wang et al. (2016) for wood-based PyOM (mean: 0.004 % day⁻¹), based primarily on lab incubation studies of PyOM addition to soils. These rates were also higher than Wang et al.'s estimate for PyOM produced within a similar pyrolysis temperature range (mean: <0.04 % day⁻¹ for PyOM produced between 200 and 550 °C). Interestingly, the mineralization rate for the water-extractable PyOM-C fraction of Py350 closely matches the mineralization rate of the "mediumDPyOM" treatment (0.29 % day⁻¹) from the Whitman et al. study (Whitman et al., 2014b), which used sugar maple PyOM produced at 325 °C. In their study, dissolved PyOM was extracted and reintroduced, and they observed an increase in cumulative PyOM-C mineralization when more dissolved PyOM was added back.

Meaningful differences also exist between equivalent water- or non-water-extractable fractions of PyOM produced at different temperatures. When we compared the C mineralization between the two different temperatures of PyOM, we observed that the mineralizability of both the Py350 water-extractable and non-water-extractable fractions was consistently higher. This indicates that C in low-temperature PyOM is more readily decomposed by microbes. This could be due to its lower aromaticity and lower degree of condensation compared to the C in the higher temperature Py550 (Keiluweit et al., 2010; Wiedemeier et al., 2015).

Interestingly, compared to SOC, microbes preferred the water-extractable PyOM-C in both Py350 and Py550. This preference over SOC can be attributed to two main factors: firstly, the difference in chemical composition of C, where water-soluble constituents of PyOM are more easily broken down by microbes compared to the more aromatic or condensed structures that are also included in the bulk SOC. It is possible that if we had compared the dissolved organic carbon (DOC) fraction of the SOC to the water-extractable PyOM-C, the DOC could potentially be more mineralizable. Secondly, since the soil was collected from a previously burned site, the microbial community may include microbes that prefer or equivalently use PyOM-C over SOC, contributing to the higher mineralizability of water-extractable PyOM-C. The identification of PyOM-responsive taxa in this study supports this understanding.

When it came to the non-water-extractable PyOM-C fractions, the non-water-extractable PyOM-C in Py350 was preferred over SOC, while SOC was preferred over Py550-C. Additionally, the non-water extractable PyOM-C in Py550 showed a lower mineralization rate (mean: 0.001 % day⁻¹) compared to the Wang et al. meta-analysis. However, for Py350, the non-water extractable PyOM-C mineralization rate was

higher (mean: 0.03 % day⁻¹). This further highlights the typically higher degrees of condensation in Py550, making the C particularly resistant to microbial breakdown. The lower mineralizability of non-water-extractable carbon in Py550 may also be attributed to a reduction in surface functional groups, like carboxyl and hydroxyl groups (Tomczyk et al., 2020), making it more challenging for microbes to break down the carbon. Additionally, certain compounds within PyOM could exert inhibitory effects on microbial activity, further reducing its mineralizability (Mukherjee et al., 2022).

4.2. Mechanisms of positive and negative priming differed over time and with PyOM temperature

The addition of Py350 caused a positive priming effect on the mineralization of SOC, while the addition of Py550 resulted in a negative priming effect (Fig. 2B). The positive priming effect of Py350 is likely due to co-metabolism/increased microbial activity, where the addition of easily mineralizable PyOM-C increases total microbial activity and accelerates the mineralization of SOC over short periods of time (DeCiucies et al., 2018; Maestrini et al., 2015; Whitman et al., 2014a). This is strongly supported by the significant positive correlation ($R^2 = 0.87$, $p < 0.001$) between the rate of water-extractable PyOM-C mineralization and the rate of SOC priming observed during the incubation (Fig. 6B). However, the high-frequency sampling afforded by our multiplexer cavity ringdown spectroscopy (CRDS) system allowed us to also detect a negative correlation between these two variables in the first 48 h ($R^2 = 0.94$, $p < 0.001$; Fig. 6A). We propose that this is likely due to substrate switching. Substrate switching occurs when microbes preferentially use the easily mineralizable PyOM-C over SOC and can explain negative priming effects in the early stages of an incubation (DeCiucies et al., 2018; Whitman et al., 2014b). The higher C mineralizability observed from both fractions of Py350 compared to SOC, particularly in the first 48 h, supports the argument that the added PyOM-C is a more favorable substrate than the existing SOC, largely driven by the most available constituents of the water-extractable fraction in Py350. This preferential usage within the first two days results in a scenario where the remaining carbon in Py350 and SOC are both readily used by microbes through the remaining incubation period, resulting in a net positive priming effect. Positive priming could also be a result of increased microbial activity due to alleviation of nutrient constraints or soil conditioning (creation of favorable microenvironments) upon PyOM addition (DeCiucies et al., 2018; Zimmerman and Ouyang, 2019).

We can rule out substrate switching as an explanation for the negative priming effect of Py550 on SOC mineralization, as no negative correlation was observed between the rate of water-extractable Py550-C mineralization and the rate of SOC priming (Fig. S4). Instead, the short-term negative priming effect may be due to inhibition, sorption of SOC on PyOM, or dilution. Inhibitory effects of Py550 on microbes (such as reduction in microbial biomass) were not investigated, but cannot be ruled out as a potential cause. Inhibition is known to occur indirectly through changes in the soil environment or directly due to toxic chemicals released upon the addition of PyOM that inhibit microbial activity (Mukherjee et al., 2022; Smith et al., 2013). However, studies investigating the impact of PyOM produced at varying pyrolysis temperatures on microbial populations have not found a significant reduction in microbial biomass with increasing pyrolysis temperature (DeCiucies et al., 2018; Li et al., 2020), making inhibition an unlikely explanation in this study. Sorption of SOC on high-porosity, high-surface-area Py550, may also contribute to the negative priming effect by making SOC less accessible to microbes (DeCiucies et al., 2018). Dilution of the SOC pool by the addition of PyOM-C, even with just a small mass of easily mineralizable C, may also decrease mineralization. In a previous study, DeCiucies et al. (2018) found that dilution contributed to 19 % of reductions in SOC mineralization observed with PyOM produced at 450 °C over the first 7 days. The high PyOM addition rate (compared to the range of addition rates in Wang et al. (2016)) and low C content in the

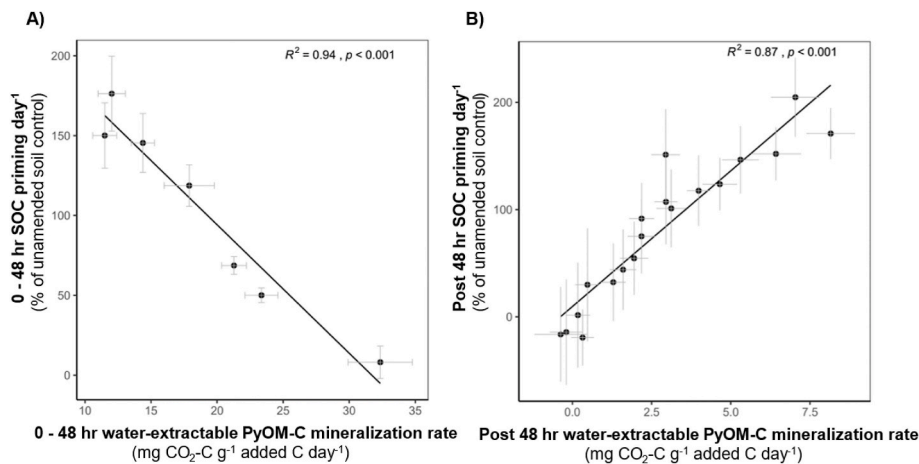


Fig. 6. Relationships between mean water-extractable PyOM-C mineralization rate and SOC priming for Py350. A) 0–48 h of soil-PyOM incubation and B) post 48 h of soil-PyOM incubation. (n = 4–5, error bars = SE). Priming calculated as: $[(\text{SOC}_{(\text{PyOM-amended})} - \text{SOC}_{(\text{unamended})}) / \text{SOC}_{(\text{unamended})}]$.

water-extractable fraction of Py550 make dilution a valid possibility in the first few days. To further understand the mechanisms behind the negative priming effect of Py550 on SOC mineralization, additional research is needed. Adsorption isotherms and high-resolution imaging of ^{13}C -labeled PyOM surface could help investigate the role of sorption in negative priming. Modifying the surface properties of PyOM and understanding its relation to sorption, as well as experiments with varying addition rates, could also be valuable in determining the relative contributions of dilution vs. sorption.

4.3. PyOM addition increased the abundance of some bacterial taxa

The addition of PyOM had a significant effect on the composition of the bacterial and archaeal community almost immediately (Fig. 3A and 3C). Given the absence of any pH effects, the shift in communities is most likely primarily a response to the C in PyOM, which can serve as a substrate for microbial growth and metabolism. The shift in communities within the first few days of PyOM addition coincides with a sharp increase in the mineralization of the water-extractable fractions in both Py350 and Py550. As PyOM-C is broken down, it creates a pool of degradation byproducts which can alter the chemical profile of soil over time. This shift was captured through the LC-MS analysis – we observed significant shifts in the chemical composition of the soil with PyOM addition, which complements the shifts in microbial community composition. Based on the PyOM-C mineralization trends from the flux data, we expected that microbes would preferentially use the water-extractable PyOM-C compounds first, leading to an increase in more complex, harder to break down compounds in the soil over time. Supporting this hypothesis, we identified four chemical features that were specific to both Py350 and Py550-amended soils and never detected in any unamended soil samples (Table S3). These features increased in relative abundance over time in the Py350-amended soils but declined over time in the Py550-amended soils (Fig. S5). The chemical formula of these features indicates that they are complex hydrocarbons, which suggests that their relative accumulation in the Py350-amended soils may be due to preferential utilization of water-extractable PyOM-C compounds. In the case of Py550, the limited availability of easily mineralizable water-extractable C could be more likely to lead to the greater use of these complex compounds by microbes. Further characterization of these features, including confirming that they are PyOM byproducts and a byproduct of microbial breakdown, is needed to gain deeper insights into microbial utilization of PyOM-C substrates.

In line with these findings, we would expect that microbes using easily mineralizable C would increase in relative abundance first, followed by microbes that have the capacity to use complex aromatic C

substrates. We observed an increase in the relative abundance of responsive OTUs belonging to the *Gemmatimonas* and *Pseudonocardia* genera after 18 days of incubation in the Py350-amended soils (Fig. 4B), coinciding with a period when the rate of water-extractable PyOM-C mineralization was low (Fig. S6). It is plausible that by this point, the most available C is already mineralized and that these bacteria are benefiting from their ability to utilize the condensed aromatic C in Py350 (Dai et al., 2017; Whitman et al., 2016). This was also evident in soils amended with Py550 – the only significant increase in relative abundance was observed for an OTU belonging to the genus *Gemmatimonas* on Day 10 (Fig. S7). Notably, the *Pseudonocardia* responsive OTU exhibited 100 % BLAST similarity to a *Pseudonocardia* lab isolate that was isolated by our group from burned soils in California on media containing PyOM produced at 350 °C. This provides further evidence for the capacity of *Pseudonocardia* to degrade the carbon present in Py350.

In contrast, responsive OTUs from the *Noviherbaspirillum* genus significantly increased in relative abundance in Py350-amended soils on Day 2 following PyOM addition (Fig. 4B). Previous incubation studies have observed an increase in the relative abundance of *Noviherbaspirillum* taxa with PyOM, which is attributed to their capacity to degrade aromatic C in PyOM (Baldani et al., 2014; Woollet and Whitman, 2020). Furthermore, *Noviherbaspirillum* species have been found to be more abundant in post-fire soils, suggesting their ability to exploit post-fire resources such as PyOM (Pulido-Chavez et al., 2023).

4.4. PyOM addition did not result in fungal community shifts

We observed no change in fungal community composition in response to the addition of PyOM (Fig. 3B and 3D). This was surprising, given that previous research has shown PyOM to impact whole community composition as well as specific fungal groups (Dai et al., 2016; Gao et al., 2021; Lehmann et al., 2011). Among the fungal responders, *Calypotryza* spp. have been identified as fire-responsive (Pérez-Izquierdo et al., 2021; Whitman et al., 2019). Their ability to thrive in post-fire soils is attributed to reduced competition from other fungi and capacity to grow on charred aromatic C. It is possible that bacteria were perhaps better able to utilize the nutrients provided by PyOM, and the effects of PyOM on fungi may only become apparent over longer durations when the easily mineralizable carbon becomes limited. This is supported in many ways by previous studies that have investigated PyOM effects on fungi. For example, Li et al. found that bacteria may be more affected by the aqueous extractable substances of PyOM which could appear over shorter durations, while fungi may be more affected by its porous nature and aromatic carbon compounds (Li et al., 2019). Yu et al. also observed that the PyOM-induced priming effect in

their study was strongly associated with the increase of certain bacteria in the first 8 days, with an increase in fungal groups not observed until day 40 (Yu et al., 2018). Liu et al. found an increase in the proportion of bacteria in fresh PyOM-amended soils, and fungi in 6-year-old PyOM-amended soils (Liu et al., 2019). Another factor that may have contributed to the lack of response in our study is the high microporosity of wood-based PyOM (Leng et al., 2021). It has been suggested that a high proportion of small sized pores in PyOM could be unfavorable for fungal growth and colonization (Li et al., 2019). Fine grinding of PyOM particles (chosen in order to ensure effective mixing and even distribution) can further increase the surface area and microporosity of PyOM (Leng et al., 2021), making it more difficult for fungi to colonize the PyOM. Additionally, sieving the soil before setting up the incubation could have affected filamentous fungi more than many bacteria (although sieving before incubations is a standard practice to homogenize soil across replicates). More research is needed to fully understand the effects of PyOM on fungal communities, including the role of time and the specific mechanisms at play. Future studies should also consider the potential impacts of PyOM surface area and porosity on fungal colonization.

Overall, the effects of PyOM on microbes are likely related to changes in nutrient provision, including both C and N. In addition to C and N, other PyOM properties that we did not examine in detail here, such as surface and electrochemical properties can also affect microbial response to PyOM (Sun et al., 2017; Yu et al., 2015). Ash content contributes to the alkalinity of the PyOM and is known to cause small changes in the microbial community composition (Dai et al., 2021). However, with our pH adjustment, the effect of ash content should be negligible compared to the effects of PyOM-C. The porous nature of PyOM helps it adsorb water, organic materials and nutrients, and provide a habitat for microbes (Dai et al., 2017; Luo et al., 2013), which could potentially affect microbial activity. Furthermore, PyOM sorption of acyl-homoserine lactone (AHL) intercellular signaling molecules can disrupt cell-cell communication among bacteria and affect C mineralization, especially in the short-term following addition of fresh PyOM (Masiello et al., 2013), which we did not examine directly. Despite these other potential factors, we anticipate that C availability will be the dominant factor controlling microbial response in a 30-day incubation.

4.5. Conclusion and implications

In this study, we demonstrated that the water-extractable carbon in PyOM comprises a small fraction of PyOM-C but exhibits disproportionately high mineralizability. We compared this fraction between high and low-temperature PyOM, highlighting differences in both its relative proportion and mineralizability. Our short-term incubation study revealed net positive priming of SOC upon Py350 addition, while the addition of Py550 resulted in a trend toward net negative priming. Our findings align with previous research (Maestrini et al., 2015), suggesting that short-term positive priming is primarily attributed to the presence of the water-extractable fraction. In our study, both the high proportion and high mineralizability of water-extractable C in Py350 compared to Py550 may have contributed to the positive priming effect. Moreover, we observed that the low-temperature Py350 exhibited overall higher C mineralizability than the high-temperature Py550, highlighting differences in C chemistry with pyrolysis temperature. These observations carry implications for post-burn soils in the case of fires where PyOM is predominantly produced at low temperatures. In such soils, the less aromatic PyOM-C constituents may undergo faster turnover immediately after deposition, potentially increasing SOC mineralization, especially in low-C soils that are more vulnerable to positive priming (Whitman et al., 2021). Conversely, in post-burn soils where PyOM is predominantly produced at higher temperatures, the slower turnover of PyOM-C turnover and the associated negative priming effects may contribute to long-term carbon persistence.

Additionally, we observed the influence of the water-extractable

fraction on soil chemical composition. While adding both Py350 and Py550 altered the soil chemical composition, the relatively higher proportion of water-extractable C in Py350 led to an accumulation of PyOM-specific compounds over time, which were indicative of complex hydrocarbons.

Lastly, our study identified that PyOM addition influenced bacterial community composition, leading to an increased relative abundance of specific bacteria that other studies have suggested are capable of degrading aromatic C compounds in PyOM. However, it remains unclear whether these bacteria in our study, and even in the field, increase due to actual consumption of PyOM-C. Techniques like DNA stable isotope probing (qSIP) (Hungate et al., 2015) with ¹³C-labeled PyOM could help identify the bacteria actively incorporating the C in PyOM, and combining SIP with metagenomics can provide further insights into the functional roles of these incorporators (Wang and Yao, 2021).

CRedit authorship contribution statement

Nayela Zeba: Conceptualization, Data curation, Formal analysis, Investigation, Methodology, Writing – original draft, Writing – review & editing. **Timothy D. Berry:** Conceptualization, Formal analysis, Investigation, Methodology, Writing – review & editing. **Monika S. Fischer:** Formal analysis, Investigation, Methodology, Writing – review & editing. **Matthew F. Traxler:** Formal analysis, Investigation, Writing – review & editing. **Funding acquisition, Methodology, Supervision, Resources.** **Thea Whitman:** Conceptualization, Formal analysis, Funding acquisition, Investigation, Methodology, Resources, Supervision, Writing – review & editing.

Declaration of competing interest

The authors declare that they have no known competing financial interests or personal relationships that could have appeared to influence the work reported in this paper.

Data availability

"The sequence data are deposited in the NCBI SRA under PRJNA986215. All other datasets are deposited on ESS-DIVE database under <https://data.essdive.lbl.gov/datasets/doi:10.15485/1985918>. All code is available at <https://github.com/nayelazeba/Chapter3>"

Acknowledgements

This work was made possible with the financial support of the United States Department of Energy through awards DE-SC0016365 and DE-SC0020351. We are thankful to Harry Read for labelling chamber design and construction; Akio Enders for 'charcoalator' design and construction; Miranda Sikora and Jamie Woollet for growing the labeled trees; Dana B. Johnson, Mengmeng Luo and Elias Kemna for help with setting up the soil-PyOM incubations; Neem Patel for help with soil collection; Kim Sparks and the Cornell Stable Isotope Laboratory for assistance with PyOM analyses; Wisconsin Department of Natural Resources for providing white pine seedlings; Center for High Throughput Computing (CHTC) for bioinformatics and data analysis (<https://chtc.cs.wisc.edu/uw-research-computing/cite-chtc.html>)

Appendix A. Supplementary data

Supplementary data to this article can be found online at <https://doi.org/10.1016/j.soilbio.2024.109328>.

References

- Abarenkov, K., Zirk, A., Piirmann, T., Pöhönen, R., Ivanov, F., Nilsson, R.H., Kõljalg, U., 2021. UNITE QIIME Release for Fungi. <https://doi.org/10.15156/BIO/1264708>.

- Baldani, J.I., Rouws, L., Cruz, L.M., Olivares, F.L., Schmid, M., Hartmann, A., 2014. The family Oxalobacteraceae. In: Rosenberg, E., DeLong, E.F., Lory, S., Stackebrandt, E., Thompson, F. (Eds.), *The Prokaryotes*. Springer Berlin Heidelberg, Berlin, Heidelberg, pp. 919–974. https://doi.org/10.1007/978-3-642-30197-1_291.
- Bengtsson-Palme, J., Ryberg, M., Hartmann, M., Branco, S., Wang, Z., Godhe, A., De Wit, P., Sánchez-García, M., Ebersberger, I., de Sousa, F., Amend, A., Jumpponen, A., Unterseher, M., Kristiansson, E., Abarenkov, K., Bertrand, Y.J.K., Sanli, K., Eriksson, K.M., Vik, U., Veldre, V., Nilsson, R.H., 2013. Improved software detection and extraction of ITS1 and ITS2 from ribosomal ITS sequences of fungi and other eukaryotes for analysis of environmental sequencing data. *Methods in Ecology and Evolution* 4, 914–919. <https://doi.org/10.1111/2041-210X.12073>.
- Berry, T.D., Creelman, C., Nickerson, N., Enders, A., Whitman, T., 2021. An open-source, automated, gas sampling peripheral for laboratory incubation experiments using cavity ring-down spectroscopy. *HardwareX* 10, e00208. <https://doi.org/10.1016/j.ohx.2021.e00208>.
- Bokulich, N.A., Kaehler, B.D., Rideout, J.R., Dillon, M., Bolyen, E., Knight, R., Huttley, G.A., Gregory Caporaso, J., 2018. Optimizing taxonomic classification of marker-gene amplicon sequences with QIIME 2's q2-feature-classifier plugin. *Microbiome* 6, 90. <https://doi.org/10.1186/s40168-018-0470-z>.
- Bolyen, E., Rideout, J.R., Dillon, M.R., Bokulich, N.A., Abnet, C.C., Al-Ghalith, G.A., Alexander, H., Alm, E.J., Arumugam, M., Asnicar, F., Bai, Y., Bisanz, J.E., Bittinger, K., Brejnrod, A., Brislawn, C.J., Brown, C.T., Callahan, B.J., Caraballo-Rodríguez, A.M., Chase, J., Cope, E.K., Da Silva, R., Diener, C., Dorrestein, P.C., Douglas, G.M., Durall, D.M., Duvallet, C., Edwardson, C.F., Ernst, M., Estaki, M., Fouquier, J., Gauglitz, J.M., Gibbons, S.M., Gibson, D.L., Gonzalez, A., Gorlick, K., Guo, J., Hillmann, B., Holmes, S., Holtes, H., Huttenhower, C., Huttley, G.A., Janssen, S., Jarmusch, A.K., Jiang, L., Kaehler, B.D., Kang, K.B., Keefe, C.R., Keim, P., Kelley, S.T., Knights, D., Koester, I., Kosciulek, T., Kreps, J., Langille, M.G.I., Lee, J., Ley, R., Liu, Y.-X., Loftfield, E., Lozupone, C., Maher, M., Marotz, C., Martin, B.D., McDonald, D., McIver, L.J., Melnik, A.V., Metcalf, J.L., Morgan, S.C., Morton, J.T., Naimye, A.T., Navas-Molina, J.A., Nothias, L.F., Orchanian, S.B., Pearson, T., Peoples, S.L., Petras, D., Preuss, M.L., Pruesse, E., Rasmussen, L.B., Rivers, A., Robeson, M.S., Rosenthal, P., Segata, N., Shaffer, M., Shiffer, A., Sinha, R., Song, S.J., Spear, J.R., Swafford, A.D., Thompson, L.R., Torres, P.J., Trinh, P., Tripathi, A., Turnbaugh, P.J., Ul-Hasan, S., van der Hoof, J.J.J., Vargas, F., Vázquez-Baeza, Y., Vogtmann, E., von Hippel, M., Walters, W., Wan, Y., Wang, M., Warren, J., Weber, K.C., Williamson, C.H.D., Willis, A.D., Xu, Z.Z., Zaneveld, J.R., Zhang, Y., Zhu, Q., Knight, R., Caporaso, J.G., 2019. Reproducible, interactive, scalable and extensible microbiome data science using QIIME 2. *Nature Biotechnology* 37, 852–857. <https://doi.org/10.1038/s41587-019-0209-9>.
- Bray, J.R., Curtis, J.T., 1957. An ordination of the Upland forest communities of Southern Wisconsin. *Ecological Monographs* 27, 325–349. <https://doi.org/10.2307/1942268>.
- Bruns, T.D., Chung, J.A., Carver, A.A., Glassman, S.I., 2020. A simple pyrocosm for studying soil microbial response to fire reveals a rapid, massive response by *Pyronema* species. *PLoS One* 15, e0222691. <https://doi.org/10.1371/journal.pone.0222691>.
- Callahan, B.J., McMurdie, P.J., Rosen, M.J., Han, A.W., A, A.J., 2016. HHS Public Access 13, 581–583. <https://doi.org/10.1038/nmeth.3869.DADA2>.
- Dai, Z., Barberán, A., Li, Y., Brookes, P.C., Xu, J., 2017. Bacterial community composition associated with pyrogenic organic matter (biochar) Varies with pyrolysis temperature and colonization environment. *mSphere* 2, e00085. <https://doi.org/10.1128/mSphere.00085-17>.
- Dai, Z., Hu, J., Xu, X., Zhang, L., Brookes, P.C., He, Y., Xu, J., 2016. Sensitive responders among bacterial and fungal microbiome to pyrogenic organic matter (biochar) addition differed greatly between rhizosphere and bulk soils. *Scientific Reports* 6, 1–11. <https://doi.org/10.1038/srep36101>.
- Dai, Z., Xiong, X., Zhu, H., Xu, H., Leng, P., Li, J., Tang, C., Xu, J., 2021. Association of biochar properties with changes in soil bacterial, fungal and fauna communities and nutrient cycling processes. *Biochar* 3, 239–254. <https://doi.org/10.1007/s42773-021-00099-x>.
- DeCicciis, S., Whitman, T., Woolf, D., Enders, A., Lehmann, J., 2018. Priming mechanisms with additions of pyrogenic organic matter to soil. *Geochim. Cosmochim. Acta* 238, 329–342. <https://doi.org/10.1016/j.gca.2018.07.004>.
- DeLuca, T.H., Gundale, M.J., Brimmer, R.J., Gao, S., 2020. Pyrogenic carbon generation from fire and forest Restoration treatments. *Front. For. Glob. Change* 3.
- Enright, D.J., Frangioso, K.M., Isobe, K., Rizzo, D.M., Glassman, S.I., 2022. Mega-fire in redwood tanoak forest reduces bacterial and fungal richness and selects for pyrophilous taxa that are phylogenetically conserved. *Molecular Ecology* 31, 2475–2493. <https://doi.org/10.1111/mec.16399>.
- Fischer, M.S., Stark, F.G., Berry, T.D., Zeba, N., Whitman, T., Traxler, M.F., 2021. Pyrolyzed substrates induce aromatic compound metabolism in the post-fire fungus, *Pyronema domesticum*. *Frontiers in Microbiology* 12.
- Fox, S., Sikes, B.A., Brown, S.P., Cripps, C.L., Glassman, S.I., Hughes, K., Semenova-Nelsen, T., Jumpponen, A., 2022. Fire as a driver of fungal diversity — a synthesis of current knowledge. *Mycologia* 114, 215–241. <https://doi.org/10.1080/00275514.2021.2024422>.
- Gao, W., Gao, K., Guo, Z., Liu, Y., Jiang, L., Liu, C., Liu, X., Wang, G., 2021. Different responses of soil bacterial and fungal communities to 3 Years of biochar amendment in an alkaline Soybean soil. *Frontiers in Microbiology* 12.
- Ghosal, D., Ghosh, S., Dutta, T.K., Ahn, Y., 2016. Current state of knowledge in microbial degradation of polycyclic aromatic hydrocarbons (PAHs): a review. *Frontiers in Microbiology* 7. <https://doi.org/10.3389/fmicb.2016.01369>.
- Hamer, U., Marschner, B., Brodowski, S., Amelung, W., 2004. Interactive priming of black carbon and glucose mineralisation. *Organic Geochemistry* 35, 823–830. <https://doi.org/10.1016/j.orggeochem.2004.03.003>.
- Hungate, B.A., Mau, R.L., Schwartz, E., Caporaso, J.G., Dijkstra, P., van Gestel, N., Koch, B.J., Liu, C.M., McHugh, T.A., Marks, J.C., Morrissey, E.M., Price, L.B., 2015. Quantitative microbial Ecology through stable isotope probing. *Applied and Environmental Microbiology* 81, 7570–7581. <https://doi.org/10.1128/AEM.02280-15>.
- Kassambara, A., 2022. Rstatix: Pipe-Friendly Framework for Basic Statistical Tests.
- Keiluweit, M., Nico, P.S., Johnson, M.G., 2010. Dynamic molecular structure of plant biomass-Derived black carbon (biochar). *Env. Sci Technol* 44, 1247–1253. <https://doi.org/10.1021/es9031419LB-PDF>.
- Keith, A., Singh, B., Singh, B.P., 2011. Interactive priming of biochar and labile organic matter mineralization in a smectite-rich soil. *Environ. Sci. Technol.* 45, 9611–9618. <https://doi.org/10.1021/es202186j>.
- Kozich, J.J., Westcott, S.L., Baxter, N.T., Highlander, S.K., Schloss, P.D., 2013. Development of a Dual-Index sequencing strategy and curation pipeline for analyzing amplicon sequence data on the MiSeq Illumina sequencing Platform. *Applied and Environmental Microbiology* 79, 5112–5120. <https://doi.org/10.1128/AEM.01043-13>.
- Lehmann, J., Joseph, S., 2012. Biochar for Environmental Management: An Introduction, Biochar for Environmental Management: Science and Technology. <https://doi.org/10.4324/9781849770552>.
- Lehmann, J., Rillig, M.C., Thies, J., Masiello, C.A., Hockaday, W.C., Crowley, D., 2011. Biochar effects on soil biota - a review. *Soil Biol. Biochem.* 43, 1812–1836. <https://doi.org/10.1016/j.soilbio.2011.04.022>.
- Leng, L., Xiong, Q., Yang, L., Li, Hui, Zhou, Y., Zhang, W., Jiang, S., Li, Hailong, Huang, H., 2021. An overview on engineering the surface area and porosity of biochar. *Sci. Total Environ.* 763, 144204. <https://doi.org/10.1016/j.scitotenv.2020.144204>.
- Li, X., Wang, T., Chang, S.X., Jiang, X., Song, Y., 2020. Biochar increases soil microbial biomass but has variable effects on microbial diversity: a meta-analysis. *Sci. Total Environ.* 749, 141593. <https://doi.org/10.1016/j.scitotenv.2020.141593>.
- Li, Y., Yang, Y., Shen, F., Tian, D., Zeng, Y., Yang, G., Zhang, Y., Deng, S., 2019. Partitioning biochar properties to elucidate their contributions to bacterial and fungal community composition of purple soil. *Sci. Total Environ.* 648, 1333–1341. <https://doi.org/10.1016/j.scitotenv.2018.08.222>.
- Liu, Z., Zhu, M., Wang, J., Liu, Xiuxia, Guo, W., Zheng, J., Bian, R., Wang, G., Zhang, X., Cheng, K., Liu, Xiaoyu, Li, L., Pan, G., 2019. The responses of soil organic carbon mineralization and microbial communities to fresh and aged biochar soil amendments. *GCB Bioenergy* 11, 1408–1420. <https://doi.org/10.1111/gcbb.12644>.
- Love, M.I., Anders, S., Kim, V., Huber, W., 2016. RNA-Seq workflow: gene-level exploratory analysis and differential expression. <https://doi.org/10.12688/f1000research.7035.2>.
- Love, M.I., Huber, W., Anders, S., 2014. Moderated estimation of fold change and dispersion for RNA-seq data with DESeq2. *Genome Biology* 15, 1–21. <https://doi.org/10.1186/s13059-014-0550-8>.
- Luo, Y., Durenkamp, M., De Nobili, M., Lin, Q., Devonshire, B.J., Brookes, P.C., 2013. Microbial biomass growth, following incorporation of biochars produced at 350 °C or 700 °C, in a silty-clay loam soil of high and low pH. *Soil Biol. Biochem.* 57, 513–523. <https://doi.org/10.1016/j.soilbio.2012.10.033>.
- Maestrini, B., Nannipieri, P., Abiven, S., 2015. A meta-analysis on pyrogenic organic matter induced priming effect. *GCB Bioenergy* 7, 577–590. <https://doi.org/10.1111/gcbb.12194>.
- Masiello, C.A., Chen, Y., Gao, X., Liu, S., Cheng, H.-Y., Bennett, M.R., Rudgers, J.A., Wagner, D.S., Zygourakis, K., Silberg, J.J., 2013. Biochar and microbial signaling: production conditions determine effects on microbial communication. *Environ. Sci. Technol.* 47, 11496–11503. <https://doi.org/10.1021/es401458s>.
- McMurdie, P.J., Holmes, S., 2013. phyloseq: an R package for reproducible interactive analysis and graphics of microbiome census data. *PLoS One* 8, e61217.
- Mukherjee, S., Sarkar, B., Aralappanavar, V.K., Mukhopadhyay, R., Basak, B.B., Srivastava, P., Marchut-Mikolajczyk, O., Bhatnagar, A., Semple, K.T., Bolan, N., 2022. Biochar-microorganism interactions for organic pollutant remediation: Challenges and perspectives. *Environ. Pollut.* 308, 119609. <https://doi.org/10.1016/j.envpol.2022.119609>.
- Oksanen, J., Simpson, G.L., Blanchet, F.G., Kindt, R., Legendre, P., Minchin, P.R., O'Hara, R.B., Solyomos, P., Stevens, M.H.H., Szoecs, E., Wagner, H., Barbour, M., Bedward, M., Bolker, B., Borcard, D., Carvalho, G., Chirico, M., Caceres, M.D., Durand, S., Evangelista, H.B.A., FitzJohn, R., Friendly, M., Furneaux, B., Hannigan, G., Hill, M.O., Lahti, L., McGlenn, D., Ouellette, M.-H., Cunha, E.R., Smith, T., Stier, A., Braak, C.J.F.T., Weedon, J., 2022. *Vegan: Community Ecology Package*.
- Pedregosa, F., Varoquaux, G., Gramfort, A., Michel, V., Thirion, B., Grisel, O., Blondel, M., Prettenhofer, P., Weiss, R., Dubourg, V., Vanderplas, J., Passos, A., Cournapeau, D., Brucher, M., Perrot, M., Duchesnay, É., 2011. Scikit-learn: Machine Learning in Python. *Journal of Machine Learning Research* 12, 2825–2830.
- Pellegrini, A.F.A., Ahlström, A., Hobbie, S.E., Reich, P.B., Nieradzik, L.P., Staver, A.C., Scharenbroch, B.C., Jumpponen, A., Anderegg, W.R.L., Randerson, J.T., Jackson, R. B., 2018. Fire frequency drives decadal changes in soil carbon and nitrogen and ecosystem productivity. *Nature* 553, 194–198. <https://doi.org/10.1038/nature24668>.
- Pérez-Izquierdo, L., Clemmensen, K.E., Strenghom, J., Granath, G., Wardle, D.A., Nilsson, M.-C., Lindahl, B.D., 2021. Crown-fire severity is more important than ground-fire severity in determining soil fungal community development in the boreal forest. *Journal of Ecology* 109, 504–518. <https://doi.org/10.1111/1365-2745.13529>.
- Pulido-Chavez, M.F., Randolph, J.W.J., Zalman, C., Larios, L., Homyak, P.M., Glassman, S.I., 2023. Rapid bacterial and fungal successional dynamics in first year

- after chaparral wildfire. *Molecular Ecology* 32, 1685–1707. <https://doi.org/10.1111/mec.16835>.
- Quast, C., Pruesse, E., Yilmaz, P., Gerken, J., Schweer, T., Yarza, P., Peplies, J., Glöckner, F.O., 2013. The SILVA ribosomal RNA gene database project: improved data processing and web-based tools. *Nucleic Acids Research* 41, D590–D596. <https://doi.org/10.1093/nar/gks1219>.
- R Core Team, 2022. R: A Language and Environment for Statistical Computing. R Foundation for Statistical Computing, Vienna, Austria.
- Reisser, M., Purves, R.S., Schmidt, M.W.I., Abiven, S., 2016. Pyrogenic carbon in soils: a Literature-based Inventory and a global estimation of its content in soil organic carbon and stocks. *Front. Earth Sci.* 4.
- Robinson, D., Hayes, A., Couch, S., 2022. Broom: Convert Statistical Objects into Tidy Tibbles.
- Santfín, C., Doerr, S.H., Preston, C.M., González-Rodríguez, G., 2015. Pyrogenic organic matter production from wildfires: a missing sink in the global carbon cycle. *Glob. Change Biol.* 21, 1621–1633. <https://doi.org/10.1111/gcb.12800>.
- Santos, F., Torn, M.S., Bird, J.A., 2012. Biological degradation of pyrogenic organic matter in temperate forest soils. *Soil Biol. Biochem.* 51, 115–124. <https://doi.org/10.1016/j.soilbio.2012.04.005>.
- Smith, C.R., Buzan, E.M., Lee, J.W., 2013. Potential impact of biochar water-extractable substances on environmental sustainability. *ACS Sustainable Chemistry & Engineering* 1, 118–126. <https://doi.org/10.1021/sc300063f>.
- Sun, T., Levin, B.D.A., Guzman, J.J.L., Enders, A., Muller, D.A., Angenent, L.T., Lehmann, J., 2017. Rapid electron transfer by the carbon matrix in natural pyrogenic carbon. *Nature Communications* 8, 1–12. <https://doi.org/10.1038/ncomms14873>.
- Taylor, D.L., Walters, W.A., Lennon, N.J., Bochicchio, J., Krohn, A., Caporaso, J.G., Pennanen, T., 2016. Accurate estimation of fungal diversity and abundance through improved Lineage-specific primers Optimized for Illumina amplicon sequencing. *Applied and Environmental Microbiology* 82, 7217–7226. <https://doi.org/10.1128/AEM.02576-16>.
- Tomczyk, A., Sokolowska, Z., Boguta, P., 2020. Biochar physicochemical properties: pyrolysis temperature and feedstock kind effects. *Reviews in Environmental Science and Biotechnology* 19, 191–215. <https://doi.org/10.1007/s11157-020-09523-3>.
- Tsugawa, H., Cajka, T., Kind, T., Ma, Y., Higgins, B., Ikeda, K., Kanazawa, M., VanderGheynst, J., Fiehn, O., Arita, M., 2015. MS-DIAL: data-independent MS/MS deconvolution for comprehensive metabolome analysis. *Nature Methods* 12, 523–526. <https://doi.org/10.1038/nmeth.3393>.
- Tu, C., Wei, J., Guan, F., Liu, Y., Sun, Y., Luo, Y., 2020. Biochar and bacteria inoculated biochar enhanced Cd and Cu immobilization and enzymatic activity in a polluted soil. *Environment International* 137, 105576. <https://doi.org/10.1016/j.envint.2020.105576>.
- Walters, W., Hyde, E.R., Berg-Lyons, D., Ackermann, G., Humphrey, G., Parada, A., Gilbert, J.A., Jansson, J.K., Caporaso, J.G., Fuhrman, J.A., Apprill, A., Knight, R., 2015. Improved bacterial 16S rRNA gene (V4 and V4-5) and fungal Internal Transcribed Spacer marker gene primers for microbial community Surveys. *mSystems* 1, e00009. <https://doi.org/10.1128/mSystems.00009-15>.
- Wang, J., Xiong, Z., Kuzyakov, Y., 2016. Biochar stability in soil: meta-analysis of decomposition and priming effects. *GCB Bioenergy* 8, 512–523. <https://doi.org/10.1111/gcbb.12266>.
- Wang, J., Yao, H., 2021. Applications of DNA/RNA-stable isotope probing (SIP) in environmental microbiology. In: *Methods in Microbiology*. Elsevier, pp. 227–267. <https://doi.org/10.1016/bs.mim.2020.11.004>.
- Westerling, A.L., 2016. Increasing western US forest wildfire activity: sensitivity to changes in the timing of spring. *Philos. Trans. R. Soc. B Biol. Sci.* 371, 20150178. <https://doi.org/10.1098/rstb.2015.0178>.
- Whitman, T., DeCicci, S., Hanley, K., Enders, A., Woolet, J., Lehmann, J., 2021. Microbial community shifts reflect losses of native soil carbon with pyrogenic and fresh organic matter additions and are greatest in low-carbon soils. *Applied and Environmental Microbiology*. <https://doi.org/10.1128/aem.02555-20>.
- Whitman, T., Enders, A., Lehmann, J., 2014a. Pyrogenic carbon additions to soil counteract positive priming of soil carbon mineralization by plants. *Soil Biol. Biochem.* 73, 33–41. <https://doi.org/10.1016/j.soilbio.2014.02.009>.
- Whitman, T., Pepe-Ranne, C., Enders, A., Koechli, C., Campbell, A., Buckley, D.H., Lehmann, J., 2016. Dynamics of microbial community composition and soil organic carbon mineralization in soil following addition of pyrogenic and fresh organic matter. *ISME J* 10, 2918–2930. <https://doi.org/10.1038/ismej.2016.68>.
- Whitman, T., Singh, B.P., Zimmerman, A., 2015. Priming effects in biochar-amended soils: implications of biochar-soil organic matter interactions for carbon storage. *Biochar Environ. Manag.* 453–486.
- Whitman, T., Whitman, E., Woolet, J., Flannigan, M.D., Thompson, D.K., Parisien, M.A., 2019. Soil bacterial and fungal response to wildfires in the Canadian boreal forest across a burn severity gradient. *Soil Biol. Biochem.* 138, 107571. <https://doi.org/10.1016/j.soilbio.2019.107571>.
- Whitman, T., Zhu, Z., Lehmann, J., 2014b. Carbon mineralizability determines interactive effects on mineralization of pyrogenic organic matter and soil organic carbon. *Environ. Sci. Technol.* 48, 13727–13734. <https://doi.org/10.1021/es503331y>.
- Wickham, H., Averick, M., Bryan, J., Chang, W., McGowan, L.D., François, R., Grolemund, G., Hayes, A., Henry, L., Hester, J., Kuhn, M., Pedersen, T.L., Miller, E., Bache, S.M., Müller, K., Ooms, J., Robinson, D., Seidel, D.P., Spinu, V., Takahashi, K., Vaughan, D., Wilke, C., Woo, K., Yutani, H., 2019. Welcome to the tidyverse. *Journal of Open Source Software* 4, 1686. <https://doi.org/10.21105/joss.01686>.
- Wiedemeier, D.B., Abiven, S., Hockaday, W.C., Keiluweit, M., Kleber, M., Masiello, C.A., McBeath, A.V., Nico, P.S., Pyle, L.A., Schneider, M.P.W., Smernik, R.J., Wiesenberg, G.L.B., Schmidt, M.W.I., 2015. Aromaticity and degree of aromatic condensation of char. *Organic Geochemistry* 78, 135–143. <https://doi.org/10.1016/j.orggeochem.2014.10.002>.
- Woolet, J., Whitman, T., 2020. Pyrogenic organic matter effects on soil bacterial community composition. *Soil Biol. Biochem.* 141, 107678. <https://doi.org/10.1016/j.soilbio.2019.107678>.
- Yao, Q., Liu, J., Yu, Z., Li, Y., Jin, J., Liu, X., Wang, G., 2017. Three years of biochar amendment alters soil physicochemical properties and fungal community composition in a black soil of northeast China. *Soil Biol. Biochem.* 110, 56–67. <https://doi.org/10.1016/j.soilbio.2017.03.005>.
- Yu, L., Yuan, Y., Tang, J., Wang, Y., Zhou, S., 2015. Biochar as an electron shuttle for reductive dechlorination of pentachlorophenol by *Geobacter sulfurreducens*. *Scientific Reports* 5, 16221. <https://doi.org/10.1038/srep16221>.
- Yu, Z., Chen, L., Pan, S., Li, Y., Kuzyakov, Y., Xu, J., Brookes, P.C., Luo, Y., 2018. Feedstock determines biochar-induced soil priming effects by stimulating the activity of specific microorganisms. *European Journal of Soil Science* 69, 521–534. <https://doi.org/10.1111/ejss.12542>.
- Zeba, N., Berry, T.D., Panke-Buisse, K., Whitman, T., 2022. Effects of physical, chemical, and biological ageing on the mineralization of pine wood biochar by a *Streptomyces* isolate. *PLoS One* 17, e0265663. <https://doi.org/10.1371/journal.pone.0265663>.
- Zeileis, A., Grothendieck, G., 2005. Zoo: S3 Infrastructure for regular and Irregular time series. *J. Stat. Softw.* 14, 1–27. <https://doi.org/10.18637/jss.v014.i06>.
- Zimmerman, A.R., Ouyang, L., 2019. Priming of pyrogenic C (biochar) mineralization by dissolved organic matter and vice versa. *Soil Biol. Biochem.* 130, 105–112. <https://doi.org/10.1016/j.soilbio.2018.12.011>.